

Mitigating Prior Shape Bias in Point Clouds via Differentiable Center Learning

¹Zhe Li, ¹Ziyang Zhang, ¹Jinglin Zhao, ¹Zheng Wang, ³Bocheng Ren, ²Debin Liu,
²Laurence T. Yang*

¹Huazhong University of Science and Technology

²Zhengzhou University

³Hainan University

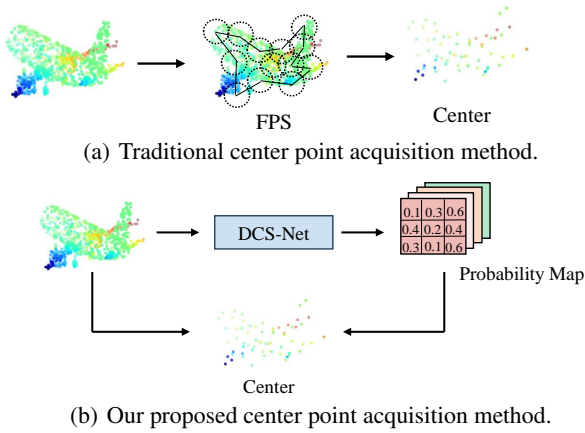


Figure 1: **Different center point acquisition methods.** (a) Conventional point cloud models employ the farthest distance sampling method for center point acquisition, resulting in trivial proxy tasks. (b) We propose a differentiable center sampling network (DCS-Net) for center point acquisition and reducing shape prior bias. By computing probability maps and weighting the points accordingly, our approach fully incorporates the semantic information of the point cloud.

Abstract

Masked autoencoding and generative pretraining have achieved remarkable success in computer vision and natural language processing, and more recently, they have been extended to the domain of point cloud modeling. Nevertheless, existing point cloud models suffer from the issue of prior shape bias due to the pre-sampling of center points, which leads to trivial proxy tasks for modeling. These approaches primarily focus on local feature reconstruction, limiting their ability to capture global patterns within point clouds. In this paper, we argue that the reduced difficulty of proxy tasks hampers the model’s capacity to learn expressive representations. To address these limitations, we introduce a novel solution called the Differentiable Center Sampling Network (DCS-Net). It tackles the prior shape bias problem by incorporating both global feature reconstruction and local feature reconstruction as non-trivial proxy tasks, enabling simultaneous learning of

both the global and local patterns within point clouds. Experimental results demonstrate that our method enhances the expressive capacity of existing point cloud models and effectively mitigates prior shape bias.

Introduction

Learning rich feature representations from unannotated data has emerged as a prominent trend in the field of deep learning, commonly referred to as self-supervised learning. This approach typically involves pretraining models on different proxy tasks and finetuning them on downstream tasks. Self-supervised learning has propelled advancements in natural language processing (Brown et al. 2020; Kenton and Toutanova 2019; Joshi et al. 2020; Liu et al. 2019; Radford et al. 2019) and computer vision (Bao et al. 2021; Chen et al. 2020a; Dosovitskiy et al. 2020; Touvron et al. 2021; Xie et al. 2021; Zhu et al. 2020) by leveraging the absence of labeled data. The ability to learn meaningful feature representations from data is attributed to the rationality of proxy tasks, such as the masked language modeling and next sentence prediction in BERT (Kenton and Toutanova 2019), as well as the masked image modeling in MAE (He et al. 2022). These proxy tasks provide valuable supervision signals that facilitate the learning of effective representations without explicit labels.

Point clouds play a pivotal role as fundamental data structures in various domains, including autonomous driving and robotics. As a result, point cloud representation learning and generation have gained escalating importance. Existing transformer-based point cloud models (Yu et al. 2022; Chen et al. 2023; Pang et al. 2022; Liu, Cai, and Lee 2022; Li et al. 2023) commonly employ the farthest point sampling (FPS) (Qi et al. 2017b) algorithm to perform center point sampling on the input point cloud, depicted in Figure 1(a). Subsequently, they leverage local feature reconstruction as a proxy task to enable the model to learn the local patterns of the point cloud, which are then finetuned in downstream tasks. However, if we perform center sampling as a separate operation before each training or fine-tuning process, it introduces unnecessary complexity and exhibits two overlooked issues: (i) **Prior Shape Bias**: the objective of the FPS algorithm is to select a set of points with the maximum average distance as the sampling result, aiming to cover the spatial range of the entire point cloud as much as possible. However, in existing

*These authors contributed equally.

point cloud models, the input is not The original point cloud but rather the center points obtained through FPS sampling. This introduces the prior shape bias as the model has prior knowledge of the approximate shape of the point cloud; (ii) **Trivial Proxy Task:** center point sampling with the FPS algorithm reduces the difficulty of model pretraining. Since the process of sampling center points is non-differentiable, the model can only use local feature reconstruction as a proxy task during pretraining, focusing solely on learning the local patterns of the point cloud while neglecting global patterns.

However, proxy tasks for pretraining should be non-trivial. By employing a differentiable approach for center point acquisition, it becomes possible to incorporate both global feature reconstruction and local feature reconstruction as proxy tasks simultaneously.

To address these challenges, we introduce DCS-Net, a differentiable center point acquisition method for point clouds depicted in Figure 1(b). This paradigm shift alters the traditional point cloud model pretraining paradigm (FPS + model pretraining), resulting in a more coherent training process and resolving the issue of prior shape bias. Specifically, we map the point cloud onto a canonical sphere, such that semantically similar parts of objects belonging to the same category are mapped to the same position. On the canonical sphere, we compute a probability map representing the likelihood of each point belonging to a certain category. By weighting all points using this probability map, we obtain the same number of centers as the number of categories. And during the model pretraining phase, we replace the FPS algorithm with DCS-Net for center sampling while keeping the subsequent operations unchanged.

Center points encapsulate rich global information of the point cloud, motivating us to design center point reconstruction as a novel proxy task for pretraining. Existing point cloud models employ unique proxy tasks, such as masked point prediction in Point-BERT and autoregressive generation in PointGPT. However, these tasks primarily focus on local feature reconstruction, overlooking the global patterns within the point cloud. By utilizing DCS-Net to acquire center points, we introduce an additional proxy task, global feature reconstruction, to complement the existing local feature reconstruction in point cloud models. This combined approach enables simultaneous learning of both global and local patterns within the point cloud. With the integration of global feature reconstruction, our method enhances the representation learning of point clouds by capturing both the fine-grained local details and the broader global structures.

To validate the effectiveness of DCS-Net, we conduct extensive experiments on various self-supervised point cloud models and multimodal point cloud models (Qi et al. 2023; Dong et al. 2022). During the pretraining process, we replace the FPS algorithm with DCS-Net for center point acquisition and simultaneously perform global feature reconstruction and local feature reconstruction tasks. The experimental results demonstrate the efficacy of our **DCS-Net+point cloud model** pretraining paradigm. Our approach not only successfully mitigates prior shape bias in the existing point cloud model but also enhances the model capacity in learning expressive representations.

Related Work

Self-supervised Learning for Point Cloud

The efficacy of self-supervised learning (SSL) in natural language processing (NLP) and computer vision has inspired researchers to extend SSL frameworks to point cloud representation learning. Among these methods, contrastive approaches (Xie et al. 2020; Zhang et al. 2021; Yang et al. 2018; Navaneet et al. 2020; Jing et al. 2020) have received considerable attention. DepthContrast (Zhang et al. 2021) generates augmented depth maps and utilizes an instance discrimination task to learn global features. Similarly, MVIF (Navaneet et al. 2020) employs cross-modal and cross-view invariance constraints to facilitate self-supervised learning of modal- and view-invariant features. Another direction of research (Dong et al. 2022; Qi et al. 2023; Xue et al. 2023a,b) aims to integrate cross-modal information and leverage knowledge transfer from language or image models to enhance 3D learning. ACT (Dong et al. 2022) introduces cross-modal autoencoders as teacher models to leverage knowledge from other modalities. Recon (Qi et al. 2023) leverages ensemble distillation to learn from both generative modeling teachers and single/cross-modal contrastive teachers. In the field of generative modeling, (Li, Chen, and Lee 2018; Achlioptas et al. 2018; Sauder and Sievers 2019; Min et al. 2022; Yu et al. 2022; Zhang et al. 2022) have made significant contributions. Point-BERT (Yu et al. 2022) employs masked point prediction as a proxy task, aiming to recover the original point tokens at the masked locations under the supervision of point tokens obtained from the tokenizer. Point-MAE (Pang et al. 2022) extends MAE by randomly masking point patches and reconstructing the masked regions. Point-M2AE (Zhang et al. 2022) further incorporates a hierarchical transformer architecture and devises corresponding masking strategies. PointGPT (Chen et al. 2023) designs a transformer-based extractor-generator with a dual masking strategy, aiming to predict the next one in an auto-regressive manner. Different from above, GPM (Li et al. 2023) proposes a new pretraining paradigm, seamlessly integrates autoencoding and autoregressive tasks in a point cloud transformer. However, these point cloud models primarily focus on training the model through local feature reconstruction, overlooking the global patterns within the point cloud. Additionally, the non-differentiability of center point acquisition has led to prior shape bias, reducing the training difficulty of the model.

Point Cloud Correspondence Learning

Given a pair of source and target instances, point cloud correspondence learning aims to find corresponding points in the target instance for each point in the source instance. Several existing methods (Chen et al. 2019a; Choy, Park, and Koltun 2019; Gojcic et al. 2019) address this task through point cloud registration, utilizing labeled pairwise correspondence as supervision. To alleviate the reliance on explicit supervision, (Bhatnagar et al. 2020) predicts part correspondences to a template using implicit functions, albeit requiring part labels for training. (Chen et al. 2020b) proposes a method for unsupervised learning of 3D dense correspondence by leveraging consistent 3D structure points across different in-

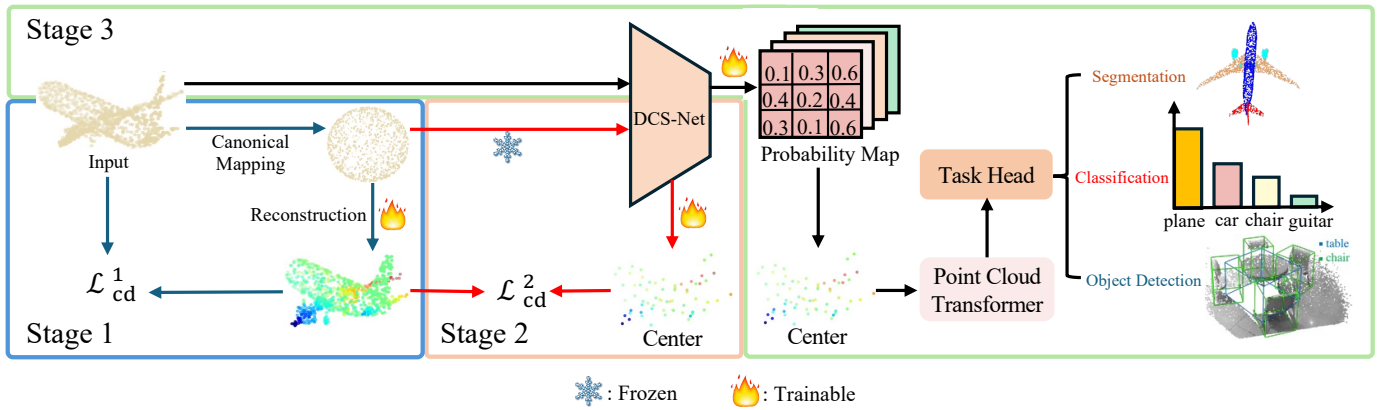


Figure 2: **Overview of DCS-Net.** We divide the entire process into three stages. Firstly, we learn a mapping function to a canonical sphere, resulting in a more uniform distribution of semantic information (represented by the blue arrows). Next, we employ DCS-Net on the canonical sphere for center point sampling, enabling the initial training of DCS-Net through center point reconstruction (represented by the red arrows). Finally, we unify the training of DCS-Net and the point cloud model by incorporating global feature reconstruction and local feature reconstruction as proxy tasks. The pretrained model is further finetuned on downstream datasets (represented by the black arrows).

stances. However, their model assumes structural similarity among instances, neglecting intra-class variations and the detection of non-existing correspondences between dissimilar shapes within the same category.

In the field of unsupervised learning, (Liu and Liu 2020) introduces an unsupervised approach that utilizes part features learned by BAE-NET (Chen et al. 2019b) to establish dense correspondences. This method can estimate a confidence score representing the likelihood of correspondence. In contrast, (Cheng et al. 2022) proposes a self-supervised correspondence learning method, which decomposes point clouds into sequences of semantically aligned shape compositions within a learned canonical space. Building upon this approach, we extract the key points of a point cloud in a canonical space with uniform semantic distribution.

The Proposed Approach

Preliminary

We aim to address prior shape bias in masked autocoding and generative models for point clouds. Existing approaches have commonly resorted to leveraging farthest point sampling as a means to pre-sample center points. However, this method inadvertently confers the model with prior knowledge regarding the approximate shape of objects, thereby diminishing the inherent challenge of training the model. In contrast, our proposed approach introduces a differentiable center point acquisition method that fully leverages the semantic information of each part of the point cloud. This method effectively resolves the prior shape bias problem and significantly enhances the overall performance of the model. Figure 2 illustrates the architecture of our proposed method.

Canonical Sphere Mapping

In order to replace the traditional FPS for center point sampling and ensure that the proxy task for model training remains non-trivial, we aim to leverage the semantic informa-

tion of different parts within the point cloud to compute the center points. However, the positions of different parts may vary for instances of one category, this can lead to semantic biases and uneven distributions.

Motivated by (Cheng et al. 2021, 2022), we initialize a mapping function $M(\cdot)$ with two MLPs that projects the point cloud onto a canonical sphere π . The canonical sphere can better capture the overall characteristics and structure of the point cloud data. By performing the reconstruction proxy task, corresponding parts of different instances in one category are mapped to the same region, effectively avoiding semantic biases. This ensures that the sphere representation reflects the inherent semantics of the point cloud data.

As depicted in Figure 3, given an input point cloud $p \in \mathbb{R}^{N \times 3}$ containing N points, we employ DGCNN (Wang et al. 2019) to encode it into a latent embedding l . Then, we replicate multiple instances of the latent embedding and connect them with points $\{x_i^\pi, y_i^\pi, z_i^\pi\}$ sampled from the canonical sphere π , as the input of the nonlinear function $F(\cdot)$, initialized with two MLPs. At the output end of the function, we reconstruct the input point cloud using the Chamfer Distance loss (Fan, Su, and Guibas 2017):

$$\mathcal{L}_{cd}^1(\mathcal{P}, \mathcal{G}) = \frac{1}{|\mathcal{P}|} \sum_{p \in \mathcal{P}} \min_{g \in \mathcal{G}} \|p - g\| + \frac{1}{|\mathcal{G}|} \sum_{g \in \mathcal{G}} \min_{p \in \mathcal{P}} \|g - p\|, \quad (1)$$

where \mathcal{P} is the ground truth point set and \mathcal{G} is the generated point set. In this way, we map the point cloud onto a canonical sphere with a more uniformly distributed semantic representation.

Point Cloud Composition Learning

Current approaches initially perform center point sampling using FPS in the point cloud. Each point is then assigned to the nearest center point, resulting in the partitioning of multiple patches. However, this approach leaks center point information during the generation process and does not consider

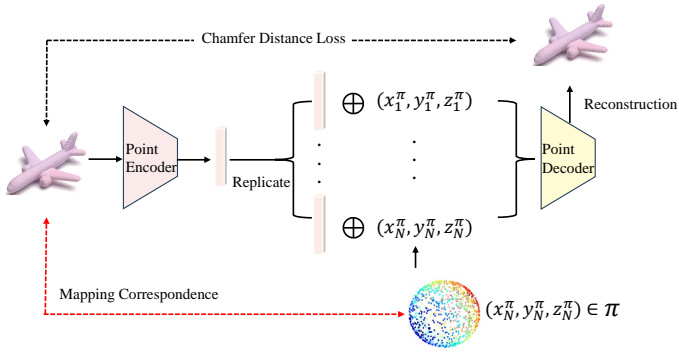


Figure 3: **Overview of canonical mapping.** It consists of two key components: a point encoder responsible for generating shape features from the input point cloud, and a nonlinear decoder function that reconstructs the input shape using the canonical sphere and the extracted shape features.

semantic prior information, often leading to discontinuous shape combinations.

To make the aforementioned process differentiable and consider the semantic information of the point cloud, we propose a differentiable approach to extract key points. The semantic information on the canonical sphere is more uniformly distributed, and the positions of points on the sphere relative to the origin, as well as the distances between them, can provide additional contextual information. Therefore, we compute a probability map $\mathcal{Q} \in \mathbb{R}^{N \times G}$ on the sphere, where G denotes the number of groups and is set as 64 for all experiments conducted. Each group is referred to as a shape composition, which can be seen as an equivalent of an image patch in the 2D domain.

Inspired by (Cheng et al. 2022), we train a self-supervised composition learning network $U(\cdot)$. For each point on the sphere, we predict its composition assignment using MLP and a Softmax activation function. This results in the probability map \mathcal{Q} of assignments for all points \hat{p} in the canonical sphere, where $\mathcal{Q}_{i,j}$ represents the probability of assigning point \hat{p}_i to the j -th group.

To ensure that the learned grouping can effectively formulate the overall semantic information of the whole point cloud, we compute h composition points $\mathcal{C} \in \mathbb{R}^{h \times 3}$ analogous to center points, where each \mathcal{C}_j is computed as follows:

$$\mathcal{C}_j = \sum_{i=1}^N M_{\pi \rightarrow p}^{-1}(\hat{p}_i) \cdot \mathcal{Q}_{i,j}, j \in \{1, 2, \dots, h\}, \quad (2)$$

we let $M_{\pi \rightarrow p}^{-1}$ denote the inverse function of $M(\cdot)$, which maps points from the canonical sphere back to the original point cloud. Then we compute the Chamfer Distance loss \mathcal{L}_{CD}^2 between the predicted center points \mathcal{C} and the ground truth point cloud \mathcal{P} :

$$\mathcal{L}_{cd}^2(\mathcal{C}, \mathcal{P}) = \frac{1}{h} \sum_{c \in \mathcal{C}} \min_{p \in \mathcal{P}} \|c - p\| + \frac{1}{|\mathcal{P}|} \sum_{p \in \mathcal{P}} \min_{c \in \mathcal{C}} \|p - c\|. \quad (3)$$

This pretraining stage makes DCS-Net undergo a warm-up process and can be directly applied in more complex point cloud spaces without operating in the canonical sphere space.

Differentiable Center Sampling Network (DCS-Net)

The reconstruction of both the global and local patterns of the point cloud should be non-trivial. To simultaneously incorporate global feature reconstruction and local feature reconstruction as proxy tasks, we employ the pretrained composition learning network $U(\cdot)$ in section as a differentiable center sampling network (DCS-Net). Moreover, we employ the Gumbel softmax relaxation (Jang, Gu, and Poole 2016) and a uniform prior for the probability map $\hat{\mathcal{Q}}$, allowing end-to-end training through backpropagation:

$$\mathcal{Q} = \text{DCS-Net}(p), \hat{\mathcal{Q}} = \text{Gumbel-softmax}(\mathcal{Q}). \quad (4)$$

Considering the crucial semantic information in each part of the point cloud, we treat $\hat{\mathcal{Q}}$ as a weight map to perform weighted operations on the points in order to obtain the center points $\hat{\mathcal{C}} \in \mathbb{R}^{G \times 3}$:

$$\hat{\mathcal{C}}_j = \sum_{i=1}^N p_i \cdot \hat{\mathcal{Q}}_{i,j}, j \in \{1, 2, \dots, G\}. \quad (5)$$

In order to realize the simultaneous learning of global pattern and local pattern in point cloud, we use global feature reconstruction and local feature reconstruction as proxy tasks. The local feature reconstruction task is handled by a subsequent point cloud model (such as the masked prediction task in GPM (Li et al. 2023)), while the global feature reconstruction task is the center reconstruction task:

$$\mathcal{L}_{cd}^3(\hat{\mathcal{C}}, \mathcal{P}) = \frac{1}{h} \sum_{c \in \hat{\mathcal{C}}} \min_{p \in \mathcal{P}} \|c - p\| + \frac{1}{|\mathcal{P}|} \sum_{p \in \mathcal{P}} \min_{c \in \hat{\mathcal{C}}} \|p - c\|. \quad (6)$$

By employing DCS-Net as a replacement for FPS to obtain center points, we successfully address prior shape problem and enable both global and local patterns learning in the point cloud with non-trivial proxy tasks. Furthermore, it is plug-and-play for all point cloud models to extract centers and devise novel proxy tasks, such as mask center prediction.

Experiment

To validate the effectiveness of DCS-Net, we conduct experiments on existing point cloud models and multimodal point cloud models, including object classification, part segmentation, few-shot learning, and transfer learning (to validate the model’s representation learning capabilities). Specifically, we replace the FPS algorithm with DCS-Net for differentiable center sampling, mitigating the issue of prior shape bias while enabling the model to learn the global pattern of the point cloud. improves the performance of the model.

Pretraining Dataset and Implementation

Following the dataset configuration similar to existing models (Yu et al. 2022; Li et al. 2023), we employ ShapeNet (Chang et al. 2015) as our pretraining dataset, encompassing over 50,000 unique 3D models spanning 55 common object categories. We sample 1024 points from the point cloud and use DCS-Net instead of the FPS algorithm for center sampling. The point cloud is divided into $G = 64$ groups, with

Methods	ScanObjectNN			ModelNet40
	OBJ_BG	OBJ_ONLY	PB_T50_RS	1k_P
<i>Self-Supervised Representation Learning</i>				
PCT (Zhao et al. 2021)	-	-	-	93.2
PointTransformer (Guo et al. 2021)	-	-	-	93.7
NPCT (Guo et al. 2021)	-	-	-	91.0
Transformer(Vaswani et al. 2017)	-	-	-	91.4
Transformer-OcCo(Vaswani et al. 2017)	-	-	-	92.1
Point-BERT(Yu et al. 2022)	87.4	88.1	83.1	92.8
Point-BERT+DCS-Net	88.1	88.8	83.2	93.4
MaskPoint(Liu, Cai, and Lee 2022)	88.4	88.0	83.8	92.9
MaskPoint+DCS-Net	88.6	88.4	84.1	93.1
Point-MAE(Pang et al. 2022)	88.9	87.6	85.1	92.7
Point-MAE+DCS-Net	89.2	88.0	85.4	92.8
PointGPT(Chen et al. 2023)	91.6	90.0	86.9	94.0
PointGPT+DCS-Net	92.3	90.8	87.1	94.3
PointM2AE(Zhang et al. 2022)	91.22	88.81	86.43	92.4
PointM2AE+DCS-Net	92.07	88.91	87.20	92.9
MaskFeat3D(Yan et al. 2023)	91.4	90.0	87.4	90.7
MaskFeat3D+DCS-Net	92.4	90.8	88.6	91.6
GPM (Li et al. 2023)	90.2	90.0	84.8	93.8
GPM+DCS-Net	90.5	90.2	85.1	94.0
<i>Methods with Cross-modal Information and Teacher Models</i>				
ACT(Dong et al. 2022)	93.3	91.9	88.2	93.7
ACT+DCS-Net	93.1	92.3	88.5	94.0
Recon(Qi et al. 2023)	95.4	93.6	91.3	94.7
Recon+DCS-Net	95.6	93.9	91.7	94.7

Table 1: **Classification results on the ScanObjectNN and ModelNet40 datasets.** The accuracy obtained on the ModelNet40 dataset is reported for 1k points. Overall accuracy (%) are reported.

each group containing 32 points. DCS-Net consists of two (convolutional layer, batch normalization layer) blocks with ReLU activation functions interspersed between them. We first pretrain DCS-Net following the guidelines in section . Then, we combine it with the point cloud model for further training, aiming to better learn the global patterns within the point cloud.

Downstream Tasks

Object Classification on Real-World Dataset. We evaluate our **DCS-Net+pretrained model** on a challenging real-world dataset ScanObjectNN dataset (Uy et al. 2019), which comprises approximately 15,000 objects extracted from real indoor scans, encompassing 2902 point clouds from 15 categories. The dataset poses a more significant challenge due to the inclusion of real-world scans with backgrounds and occlusions. Following prior work (Yu et al. 2022; Li et al. 2023; Chen et al. 2023; Pang et al. 2022), we conduct experiments on three main variants: OBJ-BG, OBJ-ONLY, and PB-T50-RS. Different from the settings in Point-MAE (Pang

et al. 2022) and PointGPT (Chen et al. 2023), we follow the configuration used in Point-BERT (Yu et al. 2022) and uniformly partition the point cloud into 64 groups. In addition to validating our approach on the classical self-supervised point cloud model, we conduct relevant experiments on two multi-modal point cloud models. From the experimental results in Table 1, it can be observed that DCS-Net not only addresses the issue of prior shape bias in traditional models but also achieves moderate improvements in the evaluation metrics. This demonstrates the effectiveness of our approach in capturing more accurate representations of the global patterns in point clouds.

Object Classification on Clean Object Dataset. We evaluate our method on the ModelNet40 dataset (Wu et al. 2015), comprising 12,311 clean 3D CAD models spanning 40 categories. Following the experimental setup of Point-BERT (Yu et al. 2022), we utilize a two-layer MLP with a dropout rate of 0.5 as the classification head for the task. The model optimization is performed using AdamW with a weight decay of 0.05 and a learning rate of 0.0005. A batch size of 32 and

Methods	5-way		10-way	
	10-shot	20-shot	10-shot	20-shot
<i>Self-Supervised Representation Learning</i>				
Point-BERT (Yu et al. 2022)	94.6 ± 3.1	96.3 ± 2.7	91.0 ± 5.4	92.7 ± 5.1
Point-BERT+DCS-Net	96.4 ± 2.7	98.2 ± 1.9	93.3 ± 5.1	95.1 ± 5.7
MaskPoint (Liu, Cai, and Lee 2022)	94.6 ± 4.1	96.8 ± 2.3	91.1 ± 4.2	92.9 ± 2.9
MaskPoint+DCS-Net	96.6 ± 2.8	98.4 ± 3.2	92.8 ± 4.9	94.6 ± 4.1
Point-MAE (Pang et al. 2022)	94.9 ± 3.4	96.8 ± 2.2	91.8 ± 3.6	94.3 ± 2.7
Point-MAE+DCS-Net	95.5 ± 3.6	98.0 ± 2.2	92.8 ± 4.2	95.1 ± 4.5
PointGPT (Chen et al. 2023)	96.8 ± 2.0	98.6 ± 1.1	92.6 ± 4.6	95.2 ± 4.3
PointGPT+DCS-Net	97.1 ± 2.3	98.4 ± 0.9	92.8 ± 4.3	95.4 ± 4.1
PointM2AE (Zhang et al. 2022)	96.8 ± 1.8	98.3 ± 1.4	92.3 ± 4.5	95.0 ± 3.0
PointM2AE+DCS-Net	97.2 ± 2.0	98.5 ± 3.7	92.8 ± 4.0	95.3 ± 3.1
MaskFeat3D (Yan et al. 2023)	97.1 ± 2.1	98.4 ± 1.6	93.4 ± 3.8	95.7 ± 3.4
MaskFeat3D+DCS-Net	97.6 ± 1.9	98.4 ± 0.9	93.8 ± 3.4	96.1 ± 3.0
GPM (Li et al. 2023)	97.0 ± 4.2	97.9 ± 3.2	92.6 ± 4.6	94.3 ± 5.4
GPM+DCS-Net	97.3 ± 4.0	98.9 ± 2.8	93.0 ± 4.7	95.1 ± 2.7
<i>Methods with Cross-modal Information and Teacher Models</i>				
ACT (Dong et al. 2022)	96.8 ± 2.3	98.0 ± 1.4	93.3 ± 4.0	95.6 ± 2.8
ACT+DCS-Net	97.0 ± 2.9	98.3 ± 1.8	93.6 ± 3.7	95.6 ± 2.4
Recon (Qi et al. 2023)	97.3 ± 1.9	98.9 ± 1.2	93.8 ± 4.0	95.8 ± 2.8
Recon+DCS-Net	97.7 ± 1.8	99.0 ± 1.0	94.0 ± 3.3	95.7 ± 2.7

Table 2: **The results of few-shot classification on the ModelNet40 dataset.** For each experimental setting, we conduct 10 independent experiments and report the average accuracy (%) along with its standard deviation.

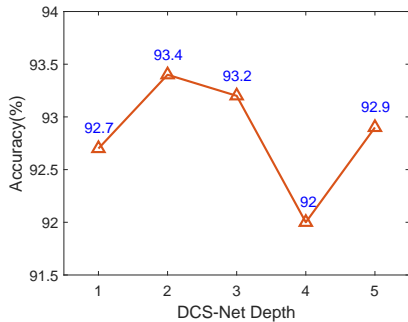


Figure 4: **Ablation study of DCS-Net depth.** The DCS-Net depth represents the ablation for classification finetune on ModelNet40 dataset. We conduct experiments with depth = {1, 2, 3, 4, 5}, and when the depth is 2, the finetuning effect is the best.

a cosine annealing schedule are employed. Additionally, we only report the accuracy achieved on the ModelNet40 dataset for 1k points. The results presented in Table 1 demonstrate that our method obtains more competitive results.

Few-shot Learning. To demonstrate the model’s ability of acquiring knowledge for new tasks with limited training data, we evaluate it in the context of few-shot learning. Following the typical ‘ W -way S -shot’ setup, we randomly select W classes and sample ($S+20$) objects for each class (Sharma and Kaul 2020). The model is then trained on $W \times S$ samples (support set) and evaluated on the remaining $20W$ samples (query set). We conduct 10 independent experiments for each setting and report the average performance and standard deviation across the 10 runs. As shown in Table 2, DCS-Net enhances the model’s generalization capability by employing both global feature reconstruction and local feature reconstruction as proxy tasks.

Methods	Cls.mIoU	Inst.mIoU
<i>Self-Supervised Representation Learning</i>		
Point-BERT (Yu et al. 2022)	84.11	85.60
Point-BERT+DCS-Net	84.24	85.60
MaskPoint (Liu, Cai, and Lee 2022)	83.4	85.1
MaskPoint+DCS-Net	84.0	85.8
Point-MAE (Pang et al. 2022)	83.6	85.66
Point-MAE+DCS-Net	84.0	85.73
PointM2AE (Zhang et al. 2022)	84.9	86.5
PointM2AE+DCS-Net	85.3	86.8
MaskFeat3D (Yan et al. 2023)	86.3	84.9
MaskFeat3D+DCS-Net	86.6	85.4
PointGPT (Chen et al. 2023)	84.1	86.2
PointGPT+DCS-Net	84.5	86.6
GPM (Li et al. 2023)	84.20	85.80
GPM+DCS-Net	84.31	86.03
<i>Methods with Cross-modal Information and Teacher Models</i>		
ACT (Dong et al. 2022)	84.7	86.1
ACT+DCS-Net	85.0	86.5
Recon (Qi et al. 2023)	84.8	86.5
Recon+DCS-Net	85.0	86.5

Table 3: **Part segmentation results on the ShapeNetPart dataset.** We report the average intersection mIoU over the union of all classes (Cls.) and instances (Inst.).

Part Segmentation. We assess the representation learning capability of our approach on the ShapeNetPart dataset (Yi et al. 2016), with the objective of predicting more fine-grained class labels for each point. This dataset comprises 16 categories and includes a total of 16,881 objects. We sample 2048 points from each model and increase the G from 64 to 128. The segmentation head (Pang et al. 2022) connects features $\mathcal{F}^4, \mathcal{F}^8, \mathcal{F}^{12}$ extracted from the 4-th, 6-th, and 12-th layers of the transformer blocks. Subsequently, average pooling, max pooling, and upsampling are employed to generate features for each point, followed by label prediction using a multi-layer perceptron (MLP). The experimental results presented in Table 3 demonstrate the superior performance of our DCS-Net.

Real-world Object detection

To validate the efficacy of DCS-Net in the context of point cloud object detection, we conduct experiments on the ONCE (Mao et al. 2021) dataset, shown in Table 4. ONCE dataset incorporates three types of coordinate systems: the LiDAR coordinate, the camera coordinates, and the image coordinate. The LiDAR coordinate system is centered at the LiDAR sensor, with the x-axis pointing to the left, the y-axis pointing backwards, and the z-axis pointing upwards. The camera coordinates can be directly converted to the LiDAR coordinate system using the respective extrinsics. The image coordinate system is a 2D system where the origin is located at the top-left corner of the image. The x-axis runs along the width of the image, and the y-axis runs along the height. The transformation from the camera coordinate to the image coordinate is achieved using the camera intrinsics.

We conduct the experiment on the PointRCNN (Shi, Wang, and Li 2019) and PV-RCNN (Shi et al. 2020). The metrics used for evaluation include mean Average Precision (mAP) on vehicle, pedestrian, cyclist and average of them. Unlike other methods that require both RGB images and point clouds

Methods	Vehicle (%)	Pedestrian (%)	Cyclist (%)	Average (%)
PointRCNN (Shi, Wang, and Li 2019)	52.09	4.28	29.84	28.74
PointRCNN+DCS-Net	62.74	10.29	35.41	32.90
PV-RCNN (Shi et al. 2020)	77.77	23.50	59.37	53.55
PV-RCNN+DCS-Net	79.63	25.60	62.92	54.39

Table 4: **Real-world object detection results on ONCE dataset.** We report the mAP (%) on vehicle, pedestrian, cyclist and average of them to validate the effectiveness of our approach.

Methods	mIOU (%)	mACC (%)	OA (%)
Point Transformer (Zhao et al. 2021)	70.4	76.5	90.8
Point Transformer+DCS-Net	70.8	77.0	91.0
StratifiedFormer (Lai et al. 2022)	71.7	77.6	91.9
StratifiedFormer+DCS-Net	72.1	77.9	92.1

Table 5: **Real-world segmentation results on S3DIS dataset.** We report the mIOU (%), mACC (%) and OA (%) as the main metric. The results show that DCS-Net can not only address the shape prior bias, but improve the performance of model on the real-world segmentation.

as inputs, PointRCNN and PV-RCNN only receive point clouds as input. Here we replace the FPS center point sampling method in the two models with DCS-Net and achieve better detection performance, thereby validating the effectiveness of DCS-Net in the real-world object detection dataset.

Real-world Segmentation

To validate the efficacy of DCS-Net in the context of real-world segmentation, we conduct experiments on the S3DIS (Armeni et al. 2016) dataset in Point Transformer (Zhao et al. 2021) and StratifiedFormer (Lai et al. 2022), the results are shown in Table 5. S3DIS dataset is utilized for semantic scene parsing, encompasses 271 individual rooms distributed across six distinct areas within three separate buildings. Each point within the scan is assigned a semantic label from one of 13 predefined categories, such as ceiling, floor, and table.

We evaluate the Point Transformer and StratifiedFormer by excluding Area 5 during the training phase and then testing on it. The metrics used for evaluation include mean class-wise intersection over union (mIoU), mean class-wise accuracy (mAcc), and overall point-wise accuracy (OA). Similar to the detection task, we replace the FPS sampling process in Point Transformer and StratifiedFormer with the differentiable center point sampling (DCS-Net), achieving moderate improvements and reducing the shape prior bias problem. The parameter settings during the experiment are consistent with those in the original paper.

Ablation Study

Hyper Parameter. Figure 4 demonstrates the ablation study on the DCS-Net depth during Point-BERT pretraining and whether to finetune the DCS-Net during the fine-tuning phase. It can be observed that the DCS-Net achieves optimal performance when the network depth is set to 2. Additionally, applying the stop-gradient operation to the DCS-Net during finetuning not only aligns with the plug-and-play requirement

but also leads to improved performance.

Reconstruction Loss. By leveraging DCS-Net to acquire center points, we enable the model to treat center reconstruction as a proxy task and learn the global patterns of point clouds. Table 6 presents the performance of variants using different center reconstruction loss functions, including $l1$ -form CD loss, $l2$ -form CD loss, Maximum Mean Discrepancy (MMD) loss, and a combination of both $l1$ and $l2$ -forms CD loss, in terms of classification results on the ModelNet40 dataset. MMD is primarily used to measure the distance between two different yet related distributions:

$$\mathcal{L}_{\text{MMD}}(S_g, S_r) = \frac{1}{|S_r|} \sum_{X \in S_r} \min_{Y \in S_g} D(X, Y), \quad (7)$$

where S_g denotes the generated set and S_r represents the query set. The function $D(X, Y)$ can either be Chamfer Distance or Earth Mover’s Distance. Moreover, we conduct many additional ablation studies and discussions in the supplementary, including reconstruction loss in canonical mapping and composition learning, whether or not freeze DCS-Net during finetuning and so on.

Model (<i>with DCS-Net</i>)	$l1$ CD	$l2$ CD	$l1+l2$ CD	MMD
Point-BERT	93.1	93.4	93.2	93.2
MaskPoint	92.7	93.1	92.9	92.4
Point-MAE	92.5	92.8	92.8	91.9
Point-M2AE	92.6	92.9	92.8	92.0
MaskFeat3D	91.4	91.6	91.4	90.8
PointGPT	92.9	93.3	93.1	92.7
GPM	93.4	94.0	93.6	93.4
Recon	93.6	94.0	93.7	93.4
ACT	94.1	94.7	94.4	94.1

Table 6: **Ablation study on the global feature reconstruction loss.** We report the accuracy achieved through finetuning on the ModelNet40 dataset.

Conclusion

In this study, we present **DCS-Net**, an innovative pretraining framework specifically designed for point cloud models, which effectively eliminates prior shape bias issue and facilitates the exploration of global patterns. DCS-Net introduces a differentiable approach to center point acquisition, which enhances the complexity of the training process. By incorporating non-trivial proxy tasks for global and local feature reconstruction, the model successfully captures both global and local patterns within the point cloud. The experimental results demonstrate that replacing the original farthest point sampling (FPS) algorithm with DCS-Net for center point acquisition not only mitigates prior shape bias in the point cloud model but also significantly improves performance in downstream point cloud tasks. This highlights the effectiveness and potential of DCS-Net in enhancing the capabilities of point cloud models for various applications.

References

- Achlioptas, P.; Diamanti, O.; Mitliagkas, I.; and Guibas, L. 2018. Learning representations and generative models for 3d point clouds. In *International conference on machine learning*, 40–49. PMLR.
- Armeni, I.; Sener, O.; Zamir, A. R.; Jiang, H.; Brilakis, I.; Fischer, M.; and Savarese, S. 2016. 3d semantic parsing of large-scale indoor spaces. In *Proceedings of the IEEE conference on computer vision and pattern recognition*, 1534–1543.
- Bao, H.; Dong, L.; Piao, S.; and Wei, F. 2021. BEiT: BERT Pre-Training of Image Transformers. In *International Conference on Learning Representations*.
- Bhatnagar, B. L.; Sminchisescu, C.; Theobalt, C.; and Pons-Moll, G. 2020. Combining implicit function learning and parametric models for 3d human reconstruction. In *Computer Vision—ECCV 2020: 16th European Conference, Glasgow, UK, August 23–28, 2020, Proceedings, Part II 16*, 311–329. Springer.
- Brown, T.; Mann, B.; Ryder, N.; Subbiah, M.; Kaplan, J. D.; Dhariwal, P.; Neelakantan, A.; Shyam, P.; Sastry, G.; Askell, A.; et al. 2020. Language models are few-shot learners. *Advances in neural information processing systems*, 33: 1877–1901.
- Chang, A. X.; Funkhouser, T.; Guibas, L.; Hanrahan, P.; Huang, Q.; Li, Z.; Savarese, S.; Savva, M.; Song, S.; Su, H.; et al. 2015. Shapenet: An information-rich 3d model repository. *arXiv preprint arXiv:1512.03012*.
- Chen, G.; Wang, M.; Yang, Y.; Yu, K.; Yuan, L.; and Yue, Y. 2023. PointGPT: Auto-regressively Generative Pre-training from Point Clouds. *arXiv preprint arXiv:2305.11487*.
- Chen, M.; Radford, A.; Child, R.; Wu, J.; Jun, H.; Luan, D.; and Sutskever, I. 2020a. Generative pretraining from pixels. In *International conference on machine learning*, 1691–1703. PMLR.
- Chen, M.; Zou, Q.; Wang, C.; and Liu, L. 2019a. Edgernet: Deep metric learning for 3d shapes. *Computer Aided Geometric Design*, 72: 19–33.
- Chen, N.; Liu, L.; Cui, Z.; Chen, R.; Ceylan, D.; Tu, C.; and Wang, W. 2020b. Unsupervised learning of intrinsic structural representation points. In *Proceedings of the IEEE/CVF conference on computer vision and pattern recognition*, 9121–9130.
- Chen, Z.; Yin, K.; Fisher, M.; Chaudhuri, S.; and Zhang, H. 2019b. Bae-net: Branched autoencoder for shape co-segmentation. In *Proceedings of the IEEE/CVF International Conference on Computer Vision*, 8490–8499.
- Cheng, A.-C.; Li, X.; Liu, S.; Sun, M.; and Yang, M.-H. 2022. Autoregressive 3d shape generation via canonical mapping. In *European Conference on Computer Vision*, 89–104. Springer.
- Cheng, A.-C.; Li, X.; Sun, M.; Yang, M.-H.; and Liu, S. 2021. Learning 3d dense correspondence via canonical point autoencoder. *Advances in Neural Information Processing Systems*, 34: 6608–6620.
- Choy, C.; Park, J.; and Koltun, V. 2019. Fully convolutional geometric features. In *Proceedings of the IEEE/CVF international conference on computer vision*, 8958–8966.
- Dong, R.; Qi, Z.; Zhang, L.; Zhang, J.; Sun, J.; Ge, Z.; Yi, L.; and Ma, K. 2022. Autoencoders as Cross-Modal Teachers: Can Pretrained 2D Image Transformers Help 3D Representation Learning? In *The Eleventh International Conference on Learning Representations*.
- Dosovitskiy, A.; Beyer, L.; Kolesnikov, A.; Weissenborn, D.; Zhai, X.; Unterthiner, T.; Dehghani, M.; Minderer, M.; Heigold, G.; Gelly, S.; et al. 2020. An Image is Worth 16x16 Words: Transformers for Image Recognition at Scale. In *International Conference on Learning Representations*.
- Fan, H.; Su, H.; and Guibas, L. J. 2017. A point set generation network for 3d object reconstruction from a single image. In *Proceedings of the IEEE conference on computer vision and pattern recognition*, 605–613.
- Gojcic, Z.; Zhou, C.; Wegner, J. D.; and Wieser, A. 2019. The perfect match: 3d point cloud matching with smoothed densities. In *Proceedings of the IEEE/CVF conference on computer vision and pattern recognition*, 5545–5554.
- Guo, M.-H.; Cai, J.-X.; Liu, Z.-N.; Mu, T.-J.; Martin, R. R.; and Hu, S.-M. 2021. Pct: Point cloud transformer. *Computational Visual Media*, 7: 187–199.
- He, K.; Chen, X.; Xie, S.; Li, Y.; Dollár, P.; and Girshick, R. 2022. Masked autoencoders are scalable vision learners. In *Proceedings of the IEEE/CVF conference on computer vision and pattern recognition*, 16000–16009.
- Jang, E.; Gu, S.; and Poole, B. 2016. Categorical Reparameterization with Gumbel-Softmax. In *International Conference on Learning Representations*.
- Jing, L.; Chen, Y.; Zhang, L.; He, M.; and Tian, Y. 2020. Self-supervised modal and view invariant feature learning. *arXiv preprint arXiv:2005.14169*.
- Joshi, M.; Chen, D.; Liu, Y.; Weld, D. S.; Zettlemoyer, L.; and Levy, O. 2020. Spanbert: Improving pre-training by representing and predicting spans. *Transactions of the association for computational linguistics*, 8: 64–77.
- Kenton, J. D. M.-W. C.; and Toutanova, L. K. 2019. BERT: Pre-training of Deep Bidirectional Transformers for Language Understanding. In *Proceedings of NAACL-HLT*, 4171–4186.
- Lai, X.; Liu, J.; Jiang, L.; Wang, L.; Zhao, H.; Liu, S.; Qi, X.; and Jia, J. 2022. Stratified transformer for 3d point cloud segmentation. In *Proceedings of the IEEE/CVF Conference on Computer Vision and Pattern Recognition*, 8500–8509.
- Li, J.; Chen, B. M.; and Lee, G. H. 2018. So-net: Self-organizing network for point cloud analysis. In *Proceedings of the IEEE conference on computer vision and pattern recognition*, 9397–9406.
- Li, Z.; Gao, Z.; Tan, C.; Li, S. Z.; and Yang, L. T. 2023. General Point Model with Autoencoding and Autoregressive. *arXiv:2310.16861*.
- Liu, F.; and Liu, X. 2020. Learning implicit functions for topology-varying dense 3d shape correspondence. *Advances in Neural Information Processing Systems*, 33: 4823–4834.

- Liu, H.; Cai, M.; and Lee, Y. J. 2022. Masked discrimination for self-supervised learning on point clouds. In *European Conference on Computer Vision*, 657–675. Springer.
- Liu, Y.; Ott, M.; Goyal, N.; Du, J.; Joshi, M.; Chen, D.; Levy, O.; Lewis, M.; Zettlemoyer, L.; and Stoyanov, V. 2019. Roberta: A robustly optimized bert pretraining approach. *arXiv preprint arXiv:1907.11692*.
- Loshchilov, I.; and Hutter, F. 2018. Decoupled Weight Decay Regularization. In *International Conference on Learning Representations*.
- Mao, J.; Niu, M.; Jiang, C.; Liang, H.; Chen, J.; Liang, X.; Li, Y.; Ye, C.; Zhang, W.; Li, Z.; et al. 2021. One million scenes for autonomous driving: Once dataset. *arXiv preprint arXiv:2106.11037*.
- Min, C.; Zhao, D.; Xiao, L.; Nie, Y.; and Dai, B. 2022. Voxel-mae: Masked autoencoders for pre-training large-scale point clouds. *arXiv preprint arXiv:2206.09900*.
- Navaneet, K.; Mathew, A.; Kashyap, S.; Hung, W.-C.; Jampani, V.; and Babu, R. V. 2020. From image collections to point clouds with self-supervised shape and pose networks. In *Proceedings of the IEEE/CVF Conference on Computer Vision and Pattern Recognition*, 1132–1140.
- Pang, Y.; Wang, W.; Tay, F. E.; Liu, W.; Tian, Y.; and Yuan, L. 2022. Masked autoencoders for point cloud self-supervised learning. In *European conference on computer vision*, 604–621. Springer.
- Qi, C. R.; Su, H.; Mo, K.; and Guibas, L. J. 2017a. Pointnet: Deep learning on point sets for 3d classification and segmentation. In *Proceedings of the IEEE conference on computer vision and pattern recognition*, 652–660.
- Qi, C. R.; Yi, L.; Su, H.; and Guibas, L. J. 2017b. Pointnet++: Deep hierarchical feature learning on point sets in a metric space. *Advances in neural information processing systems*, 30.
- Qi, Z.; Dong, R.; Fan, G.; Ge, Z.; Zhang, X.; Ma, K.; and Yi, L. 2023. Contrast with Reconstruct: Contrastive 3D Representation Learning Guided by Generative Pretraining. *arXiv preprint arXiv:2302.02318*.
- Radford, A.; Wu, J.; Child, R.; Luan, D.; Amodei, D.; Sutskever, I.; et al. 2019. Language models are unsupervised multitask learners. *OpenAI blog*, 1(8): 9.
- Sauder, J.; and Sievers, B. 2019. Self-supervised deep learning on point clouds by reconstructing space. *Advances in Neural Information Processing Systems*, 32.
- Sharma, C.; and Kaul, M. 2020. Self-supervised few-shot learning on point clouds. *Advances in Neural Information Processing Systems*, 33: 7212–7221.
- Shi, S.; Guo, C.; Jiang, L.; Wang, Z.; Shi, J.; Wang, X.; and Li, H. 2020. Pv-rcnn: Point-voxel feature set abstraction for 3d object detection. In *Proceedings of the IEEE/CVF conference on computer vision and pattern recognition*, 10529–10538.
- Shi, S.; Wang, X.; and Li, H. 2019. Pointcnn: 3d object proposal generation and detection from point cloud. In *Proceedings of the IEEE/CVF conference on computer vision and pattern recognition*, 770–779.
- Touvron, H.; Cord, M.; Douze, M.; Massa, F.; Sablayrolles, A.; and Jégou, H. 2021. Training data-efficient image transformers & distillation through attention. In *International conference on machine learning*, 10347–10357. PMLR.
- Uy, M. A.; Pham, Q.-H.; Hua, B.-S.; Nguyen, T.; and Yeung, S.-K. 2019. Revisiting point cloud classification: A new benchmark dataset and classification model on real-world data. In *Proceedings of the IEEE/CVF international conference on computer vision*, 1588–1597.
- Vaswani, A.; Shazeer, N.; Parmar, N.; Uszkoreit, J.; Jones, L.; Gomez, A. N.; Kaiser, Ł.; and Polosukhin, I. 2017. Attention is all you need. *Advances in neural information processing systems*, 30.
- Wang, Y.; Sun, Y.; Liu, Z.; Sarma, S. E.; Bronstein, M. M.; and Solomon, J. M. 2019. Dynamic graph cnn for learning on point clouds. *ACM Transactions on Graphics (tog)*, 38(5): 1–12.
- Wu, Z.; Song, S.; Khosla, A.; Yu, F.; Zhang, L.; Tang, X.; and Xiao, J. 2015. 3d shapenets: A deep representation for volumetric shapes. In *Proceedings of the IEEE conference on computer vision and pattern recognition*, 1912–1920.
- Xie, S.; Gu, J.; Guo, D.; Qi, C. R.; Guibas, L.; and Litany, O. 2020. Pointcontrast: Unsupervised pre-training for 3d point cloud understanding. In *Computer Vision—ECCV 2020: 16th European Conference, Glasgow, UK, August 23–28, 2020, Proceedings, Part III 16*, 574–591. Springer.
- Xie, Z.; Lin, Y.; Yao, Z.; Zhang, Z.; Dai, Q.; Cao, Y.; and Hu, H. 2021. Self-supervised learning with swin transformers. *arXiv preprint arXiv:2105.04553*.
- Xue, L.; Gao, M.; Xing, C.; Martín-Martín, R.; Wu, J.; Xiong, C.; Xu, R.; Niebles, J. C.; and Savarese, S. 2023a. ULIP: Learning a unified representation of language, images, and point clouds for 3D understanding. In *Proceedings of the IEEE/CVF Conference on Computer Vision and Pattern Recognition*, 1179–1189.
- Xue, L.; Yu, N.; Zhang, S.; Li, J.; Martín-Martín, R.; Wu, J.; Xiong, C.; Xu, R.; Niebles, J. C.; and Savarese, S. 2023b. ULIP-2: Towards Scalable Multimodal Pre-training For 3D Understanding. *arXiv preprint arXiv:2305.08275*.
- Yan, S.; Yang, Y.; Guo, Y.; Pan, H.; Wang, P.-s.; Tong, X.; Liu, Y.; and Huang, Q. 2023. 3d feature prediction for masked-autoencoder-based point cloud pretraining. *arXiv preprint arXiv:2304.06911*.
- Yang, Y.; Feng, C.; Shen, Y.; and Tian, D. 2018. Foldingnet: Point cloud auto-encoder via deep grid deformation. In *Proceedings of the IEEE conference on computer vision and pattern recognition*, 206–215.
- Yi, L.; Kim, V. G.; Ceylan, D.; Shen, I.-C.; Yan, M.; Su, H.; Lu, C.; Huang, Q.; Sheffer, A.; and Guibas, L. 2016. A scalable active framework for region annotation in 3d shape collections. *ACM Transactions on Graphics (ToG)*, 35(6): 1–12.
- Yu, X.; Tang, L.; Rao, Y.; Huang, T.; Zhou, J.; and Lu, J. 2022. Point-bert: Pre-training 3d point cloud transformers with masked point modeling. In *Proceedings of the IEEE/CVF Conference on Computer Vision and Pattern Recognition*, 19313–19322.

Zhang, R.; Guo, Z.; Gao, P.; Fang, R.; Zhao, B.; Wang, D.; Qiao, Y.; and Li, H. 2022. Point-m2ae: multi-scale masked autoencoders for hierarchical point cloud pre-training. *Advances in neural information processing systems*, 35: 27061–27074.

Zhang, Z.; Girdhar, R.; Joulin, A.; and Misra, I. 2021. Self-supervised pretraining of 3d features on any point-cloud. In *Proceedings of the IEEE/CVF International Conference on Computer Vision*, 10252–10263.

Zhao, H.; Jiang, L.; Jia, J.; Torr, P. H.; and Koltun, V. 2021. Point transformer. In *Proceedings of the IEEE/CVF international conference on computer vision*, 16259–16268.

Zhu, X.; Su, W.; Lu, L.; Li, B.; Wang, X.; and Dai, J. 2020. Deformable DETR: Deformable Transformers for End-to-End Object Detection. In *International Conference on Learning Representations*.